Elasticity and plasticity : foams near jamming
Siemens, A.O.N.

Cover Page

Universiteit Leiden

The handle http://hdl.handle.net/1887/21709 holds various files of this Leiden University dissertation.

Author: Siemens, Alexander Oltmann Nicolaas
Title: Elasticity and plasticity : foams near jamming
Issue Date: 2013-09-12

Rearrangement of Foams: Effects of Distance to Jamming

Under large deformations, any material will exhibit plastic behavior. In ordered systems, such plastic behavior is associated with the motion of defects, and defects are easily identified [7]. In contrast, for disordered systems, such as the foams we are studying here, but also emulsions, suspensions and granular media, there is no obvious local order, which means that the whole concept of defects does not apply. Nevertheless, these systems will undergo plastic deformations under large enough applied strains, as anyone who has ever used or played with shaving foam can attest. What happens microscopically during such plastic deformations, is that the constituent particles (grains, bubbles) experience rearrangements [21, 32, 33, 34, 35, 54, 55, 56, 57].

A wealth of work on plastic deformations in disordered media have revealed that in many cases, these rearrangements are build up from localized events, where one or more particles swap neighbors [56, 57]. For example, in the well-studied case of dry 2D foams, such localized events take the form of so-called T1 events, as shown in Fig. 5.1.
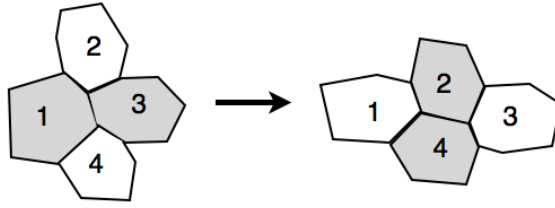
Figure 5.1 – An example of a T1 event in very dry foams. Bubbles in contact are shaded gray.

In that case, the T1 events cause most of the dissipation [57] and can organize spatially [33, 34, 55]. As a matter of fact, many other particulate systems also are believed to be dominated by T1 events (see Fig. 5.2), or by less well defined shear transformation zones [56] which are not completely localized but nevertheless have a similar quadrupolar nature.

Here we probe what happens with the nature of rearrangements in 2D foams when we start to approach the jamming point, i.e., go from the dry to the wet limit of foams. There are several reasons to expect the nature of the rearrangements to change. First, almost *any* property we probe seems to change dramatically when approaching jamming. In particular, the spatial organization of the elastic response changes from nearly affine in dry foams to strongly nonaffine in wet foams and the magnitude of the nonaffine bubble motion grows near jamming (see Sec. 5.3). In linear response, there are diverging length scales near jamming (see Sec. 2.3.1). A priori there is thus little reason to expect rearrangements to be insensitive to the distance to jamming.
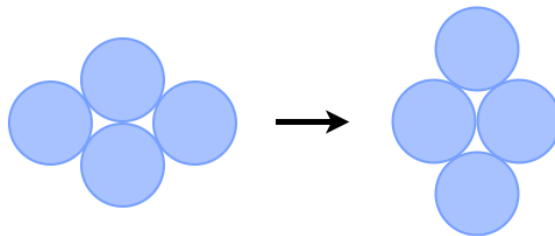
Figure 5.2 – An example of a T1 observed in many particulate systems: nearest neighbors become next-nearest neighbors.

To study rearrangements in 2D foams close and far from jamming, we will subject our foams to pure shear deformations in a so-called biaxial cell. The outline of this chapter is as follows. In Sec. 5.1 we briefly review previous work on deformations in (dry) foams. In Sec. 5.2 we describe

our experimental setup in detail. In Sec. 5.3 we describe our experiments, and show substantial qualitative trends in the nature of rearrangements as function of the J-point. We close this chapter in Sec. 5.4 with a brief discussion and suggestions for further work.

5.1 Previous Work

Studying the spatial organization (and later, rearrangements) of foams in 2D has a rich history. In 1947 Bragg et al. used bubbles floating on a free fluid surface, the so-called bubble raft, as a model for plastic failures in atomic crystalline structures such as metals [7]. By creating perfectly monodisperse bubble rafts, Bragg showed the types of dislocations and defects that arise in these structures of monodisperse bubbles. Feynman [58] noted that the slippage of a whole layer of these crystal structures in a plane does not happen in one fell swoop; rather one atom at a time moves along the slip plane. This is because it costs the system far less energy to move one particle at a time than the entire row. The same phenomenon was observed by Bragg for dislocation in the bubble rafts. Monodisperse bubble rafts thus form a simple model to probe plasticity in crystals. What about plasticity in amorphous materials?

To characterize the organization and subsequent rearrangement of bubbles in amorphous packings under small shear deformations, Argon et al. [54] used bidisperse bubble rafts. By labeling each bubble by hand, Argon could identify the number of bubbles partaking in a rearrangement and the free area change during this process. He found that dislocations due to the shear never moved the bubbles by more than 1-3 bubble diameters and that during rearrangements, these events were very localized, leaving the rest of the packing unaffected. Hence, the microscopics associated with plasticity are strongly influenced by disorder, and this work was the first indication of very localized behavior in two-dimensional foams for high packing fractions.

The 1990's saw an uptake of interest in dry foams under shear, [41, 57, 59]. An important goal was to connect the phenomenology of rearrangements to the mechanical response, i.e. stress, and to understand the role of simple shear, for instance in avalanches etc. In particular, by measuring the change in energy of their simulated bubble packing, Terwari et al. [57] observed that for dry foams there was a well-defined quasistatic limit at low enough shear rates where localized rearrangements, of T1-type, occurred at a constant rate per unit strain. Moreover, the stress response exhibited sharp downward steps whenever a rearrangement occurred. This was found to hold independent of system size. They also showed that for

wetter foams, the event size distribution broadened into a power-law that is limited by the system size. Terwari's work marked the distinctive notion that the type of rearrangements in wet and dry foams is inherently different in nature, with a more global motion occurring in wet foams and the already observed localized behavior as seen in the work of Argon being typical for dry foams [54]. [60] researched a model where the drops in stress due to a rearrangement for varying packing fractions are linked throughout a packing of bubbles, although the results are still inconclusive.

Past experimental work [32, 34, 35, 55] with bubble rafts focused on rearrangements in wet and dry foams under shear. Like the work of Terwari, Dennin's group found that the initial response of the foam is elastic and above the yield stress, it would flow. The flow in all cases consisted of irregular intervals of a build-up of stress before a sudden stress drop due to rearrangements. Simulations of these stress drops due to rearrangements in bubble rafts [61] were found to be in good agreement with the predictions of the bubble model of [55]. Furthermore, [33] found a clear correlation between the rate of T1 events and the strain rate.

5.2 Biaxial Set-up

In this section we describe the setup that we constructed in order to probe the nature of rearrangements in two-dimensional foams as function of the distance to jamming. The central part of the experiment is a biaxial cell, illustrated in Fig. 5.3. We keep our two-dimensional bidisperse foam in the central rectangular area of this cell, and an arrangement of three sliding and one fixed walls allows us to set the two dimensions, L_x and L_y, of this cell independently. Such a biaxial setup allows for a wide range of deformation experiments to be performed. In particular, by enlarging or shrinking L_x and L_y simultaneously, we can (de)compress the foam, controlling its distance to the (un)jamming point, whereas by increasing L_x whilst decreasing L_y (or vice-versa) such that the area $L_x L_y$ stays constant, we can apply a pure shear to the foam. We note here that we will only probe the spatial structure of the bubble displacements and rearrangements that take place in the foam under pure shear by imaging, and in contrast to previous chapters, will not measure the stresses arising in the foam.
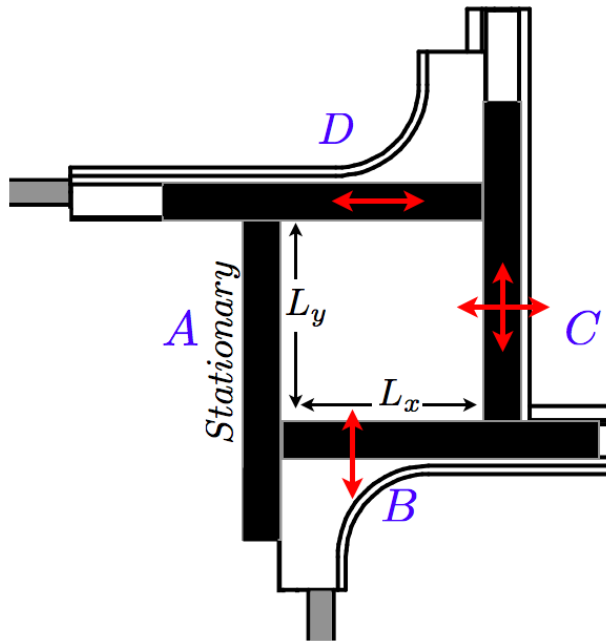
Figure 5.3 – A top view schematic of the shear cell that contains the foam packing. Wall (A) is stationary; wall (B) moves only up and down on a track connected to (A); wall (C) is connected by tracks to wall (B) and (D) and can move up/down and left/right; wall (D) can only move left and right on a track connected to (A). Walls (B) and (D) are driven by motors.

We first describe the set-up's main components and how they are put together to create the biaxial cell in Sec. 5.2.1. Sec. 5.2.2 discusses how we move the walls in order to apply a pure shear. In Sec. 5.2.3 we describe our experimental protocols, and in Sec. 5.2.4 and Sec. 5.2.5 we detail our image analysis technique.

5.2.1   Set-up
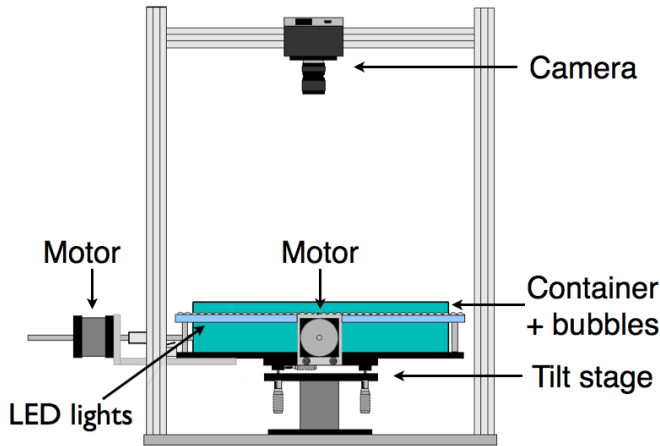
Figure 5.4 – A side view of the biaxial set-up. Two motors control the movement of the walls of a rectangular cell inside the container. The walls sit under a glass plate and bound a packing of foam bubbles confined to the cell.

Fig.5.4 and 5.5 show side and top views of our experiment. The main square container ($220 \; mm \times 220 \; mm \times 65 \; mm$) houses the soap solution and the bubbles. As before, our foam consists of a single layer of bubbles floating on a surfactant solution and trapped below a glass plate, and the main container is partially covered by a glass plate ($8 \; mm$ thick plain window glass, square of $100 \; mm \times 100 \; mm$ in dimension).

For the foam we use the same soap solutions as before (glycerol, SLES and CAPB, for details see Sec. 3.1.2). To reduce excessive use of soap solution, PMMA blocks are placed in "unused" parts of the main container, as shown in gray in Fig. 5.5. These blocks also act as barriers to decrease the thermally driven circulation of fluid in the container that is driven by heating from the lighting. We prevent evaporation of the solution by covering the top of the container not covered by the glass plate with a clear plastic square.

The shearing walls inside the container slide under the glass plate. The gap between the walls and the plate is $0.5 \; mm$ to allow the smooth motion of the walls yet still keep the packing trapped in the rectangular cell. The container sits atop a Newport M-37 Tilt and Rotation platform, which is used for leveling the system, similar as described in Sec. 3.2. The whole set-up sits on a metal framed table on which a camera is mounted. The frame is enshrouded in black cardboard to keep out the ambient light of

the room.

The lighting of the foam is crucial, since the light must strike the Plateau borders at an angle to obtain optimal contrast. The walls of the main container are made of $5\,mm$ thick, transparent PMMA, allowing light to enter the main box, and a flexible LED light-strip (Silikon LED Flexstrip from SLV Elektronik GmbH) is placed around the outside of the main container to illuminate the bubble packing inside, as shown in Fig. 5.4. The container has an anodized, black aluminum bottom plate to optimize contrast in the images.

To observe the rearrangements in the biaxial set-up, we image the foam from above with a CCD camera (Basler A101f camera with 1300×1030 pixel resolution) hung above the cell, equipped with a Cosmicar/Pentax TV lens. As the camera is straight above the center of the shear cell, we do not need to correct for skew. The camera is triggered and the images are stored using a LabVIEW code. The frame rate is fixed at $0.5\,Hz$. Distances in the image, for example to extract bubble diameters, are calibrated using $1\,mm$ spaced markings etched into the top of the shear walls as a reference length, as seen in Fig. 5.13.
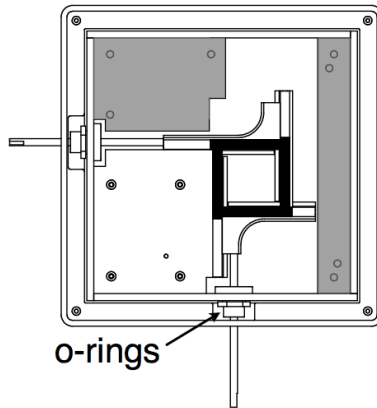
Figure 5.5 – A top view schematic of the biaxial set-up. The motor shafts are sticking out of the container.

The center of our setup are a set of moveable walls on the inside of the container that enclose the foam packing and form a biaxial cell. These walls are made of elongated, transparent PMMA rectangles, $8\,mm$ by $100\,mm$ long, which themselves are mounted on hard black, PMMA frames. These hard black frames slide perpendicular to each other by way of interlocking, swallow-tail slides and are driven by motors. A detailed view of the frames and their tracks can be seen in Fig. 5.6. Of the four bounding walls, two are

driven by the motors and three actually move. This is shown in Fig. 5.7 a). Two of the PMMA walls have cut-outs in them to allow access to the biaxial cell containing the bubbles with syringe needles, shown in Fig. 5.7 b).

The motion of the walls is controlled by stepper motors, placed outside the fluid container, that are connected to the movable wall via rods that slide through two holes in the side walls of the container (Fig. 5.4). These holes are sealed with two rubber o-rings, one on the inside and one on the outside of the container, shown in Fig. 5.5. The o-rings create a tight fit around the motor shafts and ensure that no solution leaks out. Some tuning is in order to optimize the tightness of the fit: a too-tight fit creates stick-slip motion when the motors are driving the shafts, causing the inside walls to vibrate, while too loose fits lead to leakage. We have been able to machine the o-rings such that the container remains sealed whilst allowing the shafts to move smoothly when driven. In addition, we have carefully aligned the motor shafts so as to avoid stick slip motion to occur.
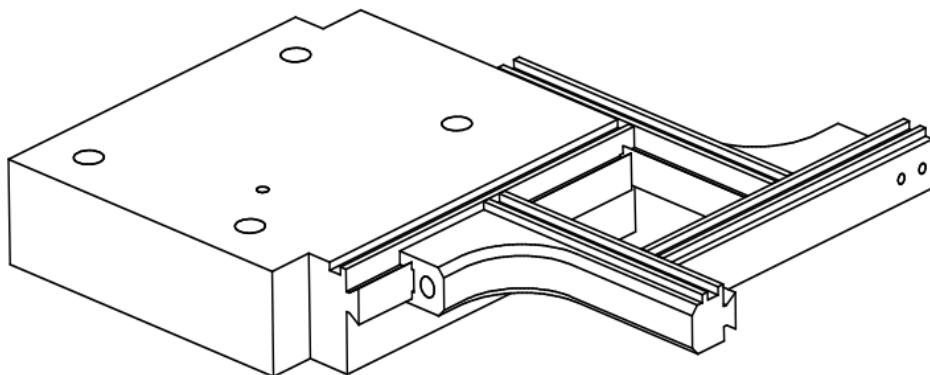
Figure 5.6 – A detailed schematic of the frames that are driven by the motors. The four foam-bounding, clear PMMA walls are mounted on these frames, which slide on swallow-tail tracks.

The motors that drive the frames (and therefore the walls) are stepper motors from Haydon Switch & Instrument Inc. A threaded shaft is translated by the rotation of the internal rotors, where each full rotation translates the shaft $0.6\,mm$. The actual control is done using a "Step Motor Ministep Driver" (model SMD41B3 by JVL Industri Elektronik) driver. This driver enables us to subtend each step into 3200 ministeps every time it receives a signal greater than $5\,V$. One step in this mode corresponds to a $186\,nm$ shift in the walls. Each motor is controlled separately by its own driver, which is provided by a $5\,V$ square wave signal made with a function generator (TTi TG1010A). The function generator is connected by GPIB

cable to a computer running a LabVIEW code from which we set the drive frequency of the signal and thus adjust the step-rate and amount by which the walls move.
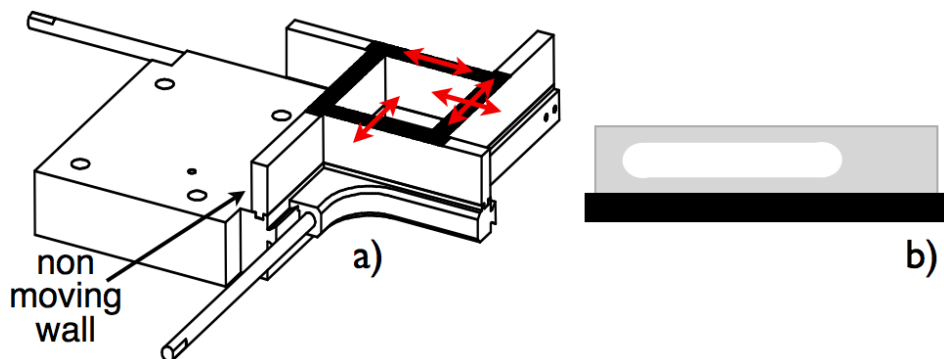
Figure 5.7 – a) A schematic of the walls and their motion, indicated by the red arrows. The walls are mounted on black, PMMA frames which are connected to the motor shafts. Only one of the four walls does not move at all. b) A side view schematic of one of the two walls and the hole through which the syringe needle to make the foam packing is placed.

The foam is made directly in the cell by placing a syringe needle through one of the cut-outs in the moveable walls. We blow N_2 gas at a constant rate through a needle submerged $2\,cm$ deep in the solution. The base pressure of the gas is $3.5\,bar$, but decreased and tuned to useable levels using valves. To control the two different bubble sizes, we use two different gauge needles, 25G and 30G ($0.26\,mm$ and $0.16\,mm$ inner diameters, respectively). We create about 50% big bubbles and 50% smaller bubbles by number. The foam bubbles we use are between $1.8 - 2.7\,mm$ in diameter, determined by image analysis. Using a bent syringe needle, as described in Sec. 3.1.2, we remove the satellite bubbles and mix the packing to ensure the bidisperse foam does not have significant crystalline patches.
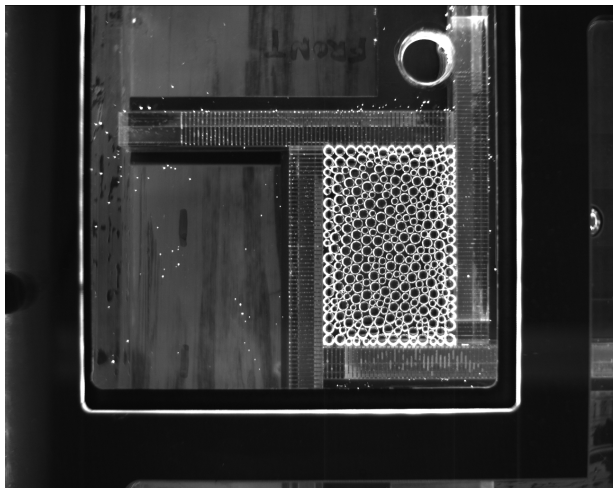
Figure 5.8 – Top view of the shear cell. The black frame holds the glass plate under which the bubbles are trapped. The motor shafts, which can not be seen, enter the set-up from the top and the right in the image. The three screws holding the frame in place are just out of the image.

5.2.2 Shear and Strain

Under shear deformations, the foam area is conserved and the foam thus remains at a similar distance to the jamming point, making shear deformations ideally suited for studies of rearrangements at controlled packing fraction. In simple shear, a single wall moves in parallel to its opposite wall, but it is hard to change or control the packing fraction. We therefore opt for using a biaxial cell. To shear foams in such a cell, we need to apply pure shear, where two boundaries move, compressing and expanding the foams in perpendicular directions as illustrated in Fig. 5.9.
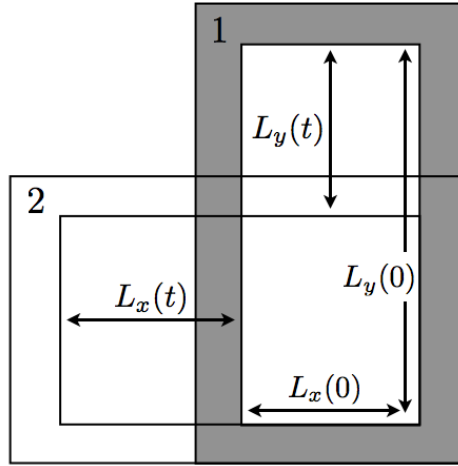
Figure 5.9 – Pure shear of a rectangle. The area under this type of shear is conserved. The rectangle starts the shear at 1 and ends in a configuration like in 2.

An experimental difficulty is that this necessitates one sidewall getting shorter, while a perpendicular wall gets longer. We resolve this by having sliding walls. Recall that in our experiment the motion of the sidewalls, and hence L_x and L_y, are controlled by the frequency of the pulse signal sent to the stepper motors. In order to keep the area $L_x L_y$ constant, we have to continuously update these driving frequencies. We will now derive the equations that dictate the speed at which the motors must move, starting from some initial position.

Consider the starting length of our X and Y walls to be $L_x(0)$ and $L_y(0)$, respectively, like in Fig. 5.9. In our experiment we drive the Y wall at a constant frequency, f_y, leading to a constant speed of the Y wall, v_y: $L_y(t) = L_Y(0) + v_y t$. Now, requiring that the area remains constant implies

$$L_x(t) = \frac{L_x(0)L_y(0)}{L_y(0) + v_y t}. \tag{5.1}$$

which upon differentiating, using $L_x(t) = L_x(0) + v_x(t)$ (we thus define outward motion for v_x as positive) and $v_{x,y} = a f_{x,y}$, where $a = 186\ nm$, yields that

$$f_x(t) = \frac{L_x(0)L_y(0)f_y}{(L_y(0) + a f_y t)^2} \tag{5.2}$$

We use LabVIEW to send this continuously varying drive frequency to the stepper motor which controls the X wall. An example of the updating signal is shown in Fig. 5.10
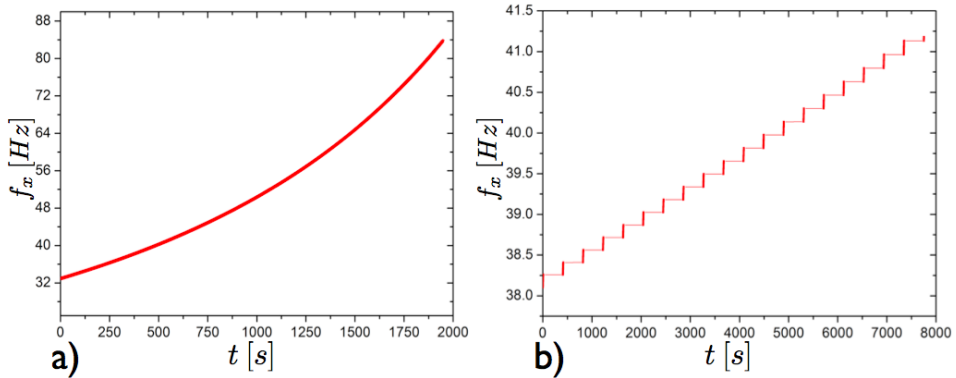
Figure 5.10 – The change of the X wall frequency, f_x, over the course of the a) continuous shear protocol and b) the "start/stop" shear protocol, where $t_c = 8$ seconds and $t_s = 400$ seconds.

We have checked that with this protocol the area under shear is indeed constant. We use ImageJ to calculate the area of the cell every 125 seconds over the course of an experiment. In Fig. 5.11 we note that even over long periods of time, the area remains constant, with very little fluctuation. The motors are thus correctly driving the system. Small deviations from a uniform area signal over the course of a run in Fig. 5.11 come from the way we manually measure the area using ImageJ.

The strain under pure shear in the biax set-up is determined by first defining a deformation $e = \frac{L_x(t) - L_x(0)}{L_x(0)}$. The lengths of the walls are therefore

$$L_x(t) \quad = \quad (1 + e)L_x(0)$$

and

$$L_y(t) = (\frac{1}{1+e})L_y(0),$$

which guarantees that $L_x(t)L_x(t) = L_x(0)L_y(0)$. We describe the initial configuration of the rectangle with the vectors $\vec{L_1} = (L_x(0), 0)$ and $\vec{L_2} = (0, L_y(0))$. After a deformation e, the new values of $\vec{L_1}$ and $\vec{L_2}$ are given by $\vec{L_i} = \overleftrightarrow{F}\vec{L_i}$, where $i = 1, 2$ and $\overleftrightarrow{F}$ is the "deformation gradient",

$$\overleftrightarrow{F} = \begin{pmatrix} 1+e & 0 \\ 0 & \frac{1}{1+e} \end{pmatrix}.$$

We use the Green strain tensor [62]
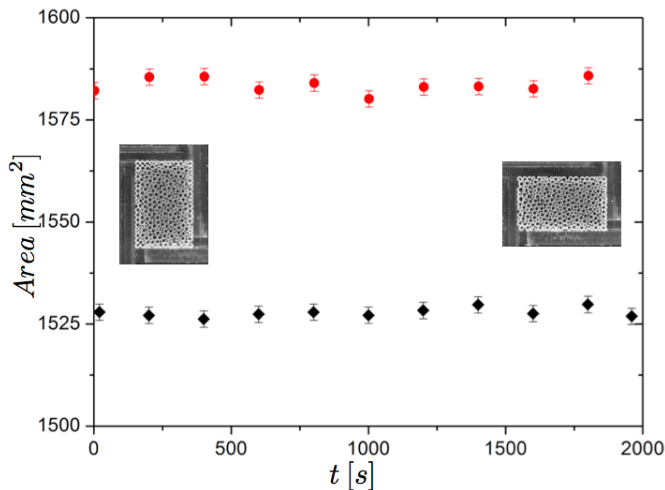
Figure 5.11 – The area of the cell as a function of time for two continuous shear runs, outlined in Sec. 5.2.3. The area remains constant over long periods of time, which is the essence of pure shear. The inset figures show how the cell looks like at $t = 0$ and $t = 2000$ seconds.

$$\overleftrightarrow{E} = \frac{1}{2}(\overleftrightarrow{F^T}\overleftrightarrow{F} - \vec{1}),$$

where $\vec{1}$ is the identity matrix. Expanding and keeping only leading order terms in e, the strain, γ, becomes

$$\gamma = \begin{pmatrix} e & 0 \\ 0 & -e \end{pmatrix},$$

which is the familiar expression for a simple pure shear strain in linear response.

5.2.3 Protocols

In this section we describe the pure shear protocols we use to probe the motion and rearrangements of bubbles in our two-dimensional foam packing. The main idea is to shear the foam either continuously or by using a start/stop-type shear. The packing fraction of the foam can be set by adjusting the dimensions of the cell, and a wet or a dry foam is created by making the cell larger or smaller, respectively. Experiments can be repeated many times, since the walls can be driven back to the same initial position after each run.

Packing Fraction – Since we shear at constant area, the foam will be completely bounded at all times in the biaxial set-up, counter to what we saw in Chapter 3. We estimate the packing fraction in our system by slowly driving one wall outwards while keeping the other three fixed until the packing falls apart.. Taking Fig. 5.9 as a reference, we drive only the X wall at a very low speeds, typically around $4.65 \times 10^{-6} \, ms^{-1}$. The low drive speed is needed to ensure the system responds quasi-statically to the change in area and that the bubbles keep up with the movement of the wall, since they are retarded by the drag with the glass plate. We make an estimate as to how far from the jamming point our foam packings are. The area of the undeformed bubbles is A_0. If the packing in the rectangle has a starting area A, then its packing fraction is $\phi = A_0/A$. We say the bubble packing falls apart at area A', so its packing fraction is $\phi' = A_0/A' = \phi_c$, the critical packing fraction. Putting these two equalities together, we get the starting packing fraction of the foam as $\phi = \phi_c \frac{A'}{A}$. The distance to the jamming point is thus found to be

$$\Delta\phi = \phi - \phi_c = \phi_c \left(\frac{A'}{A} - 1 \right). \tag{5.3}$$

Additionally, it must be noted that there is a non-trivial upper limit to the packing fraction we can achieve in the shear set-up. Starting at packing fractions of around $\Delta\phi \gtrsim 0.55$, the bubbles buckle out of plain and start creating bilayer patches of bubbles, as seen in Fig. 5.12. This happens to mainly smaller bubbles in the packing, when they are forced downward by two neighboring larger bubbles.
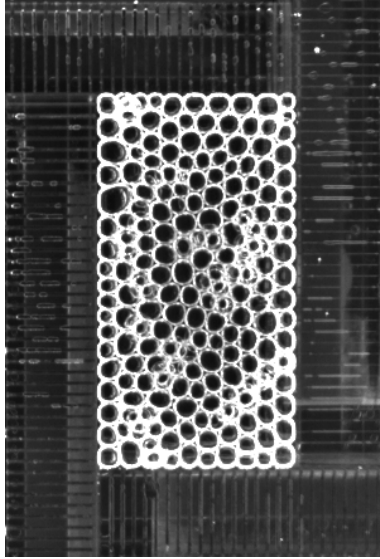
Figure 5.12 – An top view example of a highly compressed foam with bubbles that have buckled out of plane, creating a bilayer in some areas.

This upper limit of $\Delta\phi$ is therefore the driest possible achievable foam packing.

5.2.3.1   Continuous Shear Protocol

We shear the foam continuously from some initial configuration to a final position, like in Fig. 5.13. For these runs we set $v_y = 9.3 \times 10^{-6} \ ms^{-1}$ ("fast") or at $v_y = 9.3 \times 10^{-7} \ ms^{-1}$ ("slow") and the packing fraction for every run. We only shear the system in one direction. These continuous shear protocols take around 30 minutes to 4 hours to perform, which means they can be repeated many times if necessary.

5.2.3.2   Start/Stop Protocol

The second protocol is similar to the continuous protocol in that we set v_y and $\Delta\phi$ for each run. However, instead of shearing continuously, we start and stop the shear. We call this the "start/stop" protocol. By changing the output signal the motors receive, we drive the walls for a time t_c at $v_y = 9.3 \times 10^{-6} \ ms^{-1}$ and then stop them, allowing the system to sit still for time t_s. Fig. 5.10 b) highlights how f_x changes over the course of a start/stop protocol. The change in the start value of f_x seen in Fig. 5.10 comparing the continuous and start/stop protocol, or between any run for

Start

End
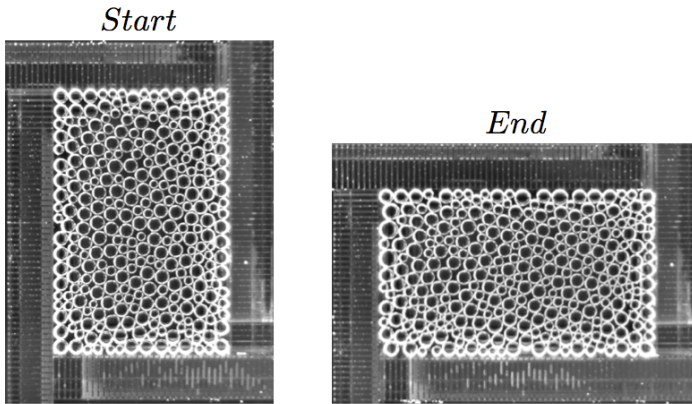
Figure 5.13 – A top view of the start and end images of a packing using the continuous shear protocol. The millimeter markings on the walls are clearly seen.

that matter, comes from the fact that there is a size dependence of the initial size of the cell in Eq. 5.2.

This cycle of starting and stopping the walls is repeated more than 50 times. The most commonly used change times were $t_c = 2, 8, 20$ seconds and sit times of $t_s = 200, 400$ seconds. The sit times are obviously a lot longer than the change time to let the foam relax after the shear and allow us to capture the motion. For wet foams, the rearrangement times are longer than for dry foams, necessitating these long sit periods. For a $t_c = 20$ seconds, $t_s = 400$ seconds is needed to ensure the system is fully relaxed. For the majority of experiments we used the combination of $t_c = 8\,s$ and $t_s = 200\,s$.

5.2.4 Affine Deformation and Variance

In order to understand what type of rearrangement is present in the packing, we analyze the images of the packing taken from above. By comparing sets of images to each other, we get a variance signal whose features tells us the changes taking place in the packing with pixel accuracy. To extract a variance signal from the images in the continuous protocol case, we first need to subtract the affine motion of the moving walls between frames, similar to what was done in Sec. 4.4.1 with the compression experiment. The bubbles at the boundary of the cell are the ones that feel the continuous motion of the walls the most and will thus show a greater change in motion between images. The rearrangements which occur in the packing will also be washed out by the motion of the walls when comparing two images. We
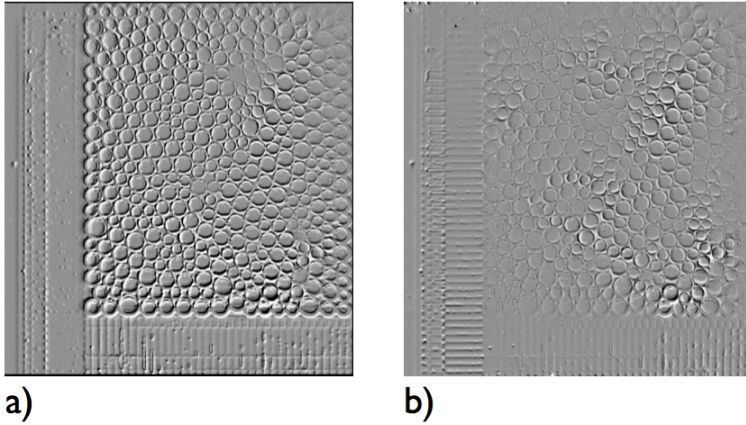
Figure 5.14 – a) In the uncorrected image, the motion of the wall's influence on the bubbles can clearly be seen during the shearing between two frames. b) The affine corrected image suppresses the motion of the walls, allowing to clearly observe details from affine motion.

correct for this in this section.

This correction process will not have to be done with the "start/stop" protocol, as we observe the rearrangements in the packing during time t_s as a response to the the walls having just sheared the packing for time t_c. In t_s we are observing how the system relaxes and accommodates the induced shear.

To remove the motion of the walls, we use the same IDL routines from Sec. 3.1.4 and Sec. 4.4.1, POLYWARP and POLY_2D. For the biaxial set-up, we first define the four coordinates of the vertices in the first image (x_j, y_j), where $j = 1, 2, 3, 4$, of the cell containing the foam. We image the pure shear of the cell with a fixed frame rate of $0.5 \, Hz$, and knowing the velocity of the Y and that the X wall speed goes like $v_x = a \times f_x$, where f_x is given by Eq. 5.2, this gives us the new coordinates (x'_j, y'_j) of the cell for each frame in the recording. The original coordinates are input into POLYWARP to extract warping coefficients. The routine POLY_2D then affinely deforms an image I_i to the affine predicted deformation at a shifted time I_{i+sh}. We refer to this affine prediction as $\bar{I}_i$.

The rearrangements are more exposed in this manner, as can be seen in Fig. 5.14 a), where we compare two images, one corrected for the affine motion of the walls, the other not.

The variance is defined similarly to Eq. 4.17, so

$$Var[sh] := \frac{\sum\limits_{i} [I_i - \bar{I}_i]^2}{\text{no. of pixels}} \, ,$$

in arbitrary units, and where a value of zero means no change has happened between images, and the larger the value, the more has changed. Because we have the coordinates of the vertices of the cell in each frame, we measure the variance only within these coordinates for each frame. Recall that the area of the cell does not change over the course of the experiment (as can be seen in Fig. 5.11), so the variance signal will not grow due to change in area of the cell, only due to the rearrangements. When comparing the corrected to the uncorrected image in Fig. 5.14, the variance signal will overall be less noisy and therefore lower with the corrected image.

5.2.5 Stick-slip in the Set-up

In the biaxial set-up, the walls of the cell exhibit stick-slip motion due to friction between the motor shafts passing through the o-rings (seen in Fig.5.5). As the shafts are pushed/pulled during a run, the stick-slip causes the walls to periodically jump forward or backward, following the overall direction of the wall's motion.

In difference images such as Fig. 5.15 a), this jump is noticeable at the boundaries of the cell. Fig. 5.15 b) shows the next difference image, directly after the jump, where no motion at the boundaries is seen. Note that both images are "corrected" for the affine, continuous motion of the walls; the sudden jumps can not be accounted for, as their occurrence is not controlled.

a)   b)
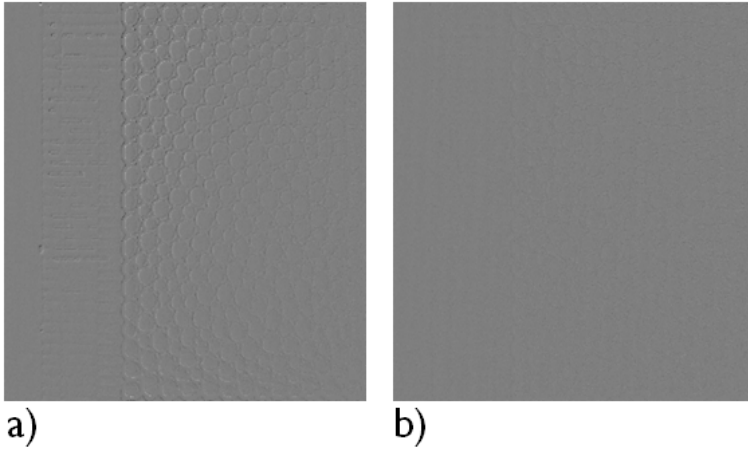
Figure 5.15 – a) The stick-slip motion of the walls causes a noticeable signal at the boundaries of the cell. b) One image later than a), the jump is not seen anymore. The stick-slip is periodic.

Because of these periodic kicks registered at the boundaries in the image analysis, the variance signal exhibits small, periodic peaks, as seen by the black data points in Fig. 5.16. These peaks mask the underlying motion and phenomenology of the variance signal and need to be corrected for. The algorithm that we use to detect unwanted peaks in the signal is illustrated in Fig. 5.17. For simplicity, let's denote the data by $Var[i]$. We then define a "smoothed" signal sm, as

$$sm[i] := \frac{Var[i-1] + Var[i+1]}{2}.$$

As we sample the data at a high rate, we do not expect very rapid, and isolated, changes in the data. However, the stick-slip motion precisely leads to signal points being systematically larger than their neighbors, i.e. $Var[i] \gg sm[i]$.

To identify the peaks only due to the walls' jumping (and spare the rest of the peaks corresponding to actual rearrangements from the averaging), we say that if $Var[i] > 1.2 \times sm[i]$, we have detected "bad" points, indicated by the blue vertical lines in Fig. 5.16. The factor 1.2 is chosen so as to suppress "real peaks" as little as possible while detecting the "false" peaks. With the "bad" point due to the wall jump identified, we replace $Var[i]$ by its neighbors average $sm[i]$, see Fig. 5.17 b). The result is the red curve in Fig. 5.16, which captures the data very well, removes the periodic stick-slip motion and shows that rearrangements (at frame 220 and 280, for example) have not been removed by this procedure.
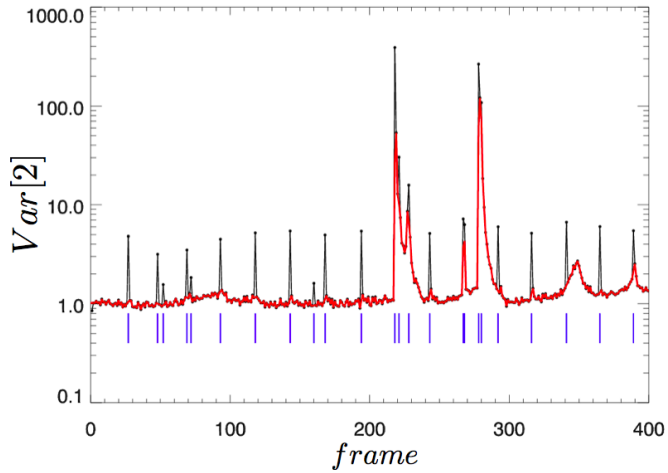
Figure 5.16 – A plot of $Var[2]$ versus frame for a run with $\Delta\phi = 0.118$. The black points are the original data, with the periodic jumps due to the wall motion. The red curve is a processed data set using a peak detection technique. The blue vertical lines indicate where peaks were detected and data points have been replaced by the average of their neighbors.
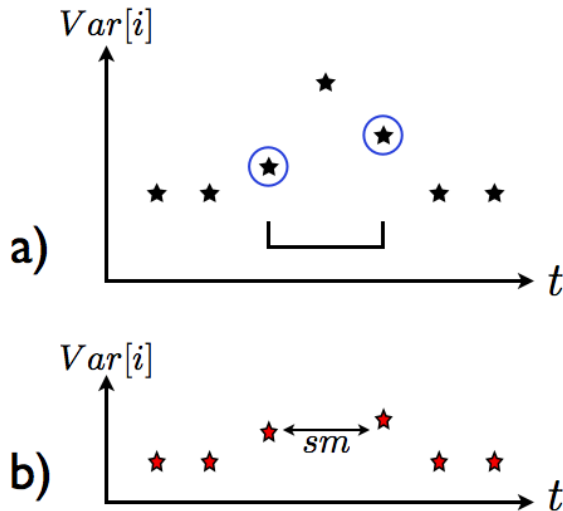
Figure 5.17 – a) Schematic of the variance signal with a high valued, "bad" point due to the stick-slip of the wall motion. The signal is averaged over three consecutive points at a time, resulting in a smoother signal as in b).

106

5.3   Results

Employing both continuous and start/stop protocols (with emphasis on the former), we will characterize the spatial structure of the rearrangements in our two-dimensional foams as a function of the packing fraction ϕ. In particular, we will employ the variance signal (see Eq. 4.17), spatial snapshots as well as the *inverse partition ratio* to capture the trends with ϕ. We find that in dry foam, rearrangements tend to be relatively short and intense. These are classical T1 events, marked by the quadrupolar nature of the deformation field during rearrangements, see Fig. 5.18. Such T1 events become less well-defined when we move away from the very dry limit. Below $\Delta\phi \approx 0.1$ they are almost irrelevant. In that regime, rearrangements are more smeared out in both space and time. In addition, for wet foams we observe that during shear "rattlers" are generated – loose particles, that with little interaction with their neighbors move in their cage.
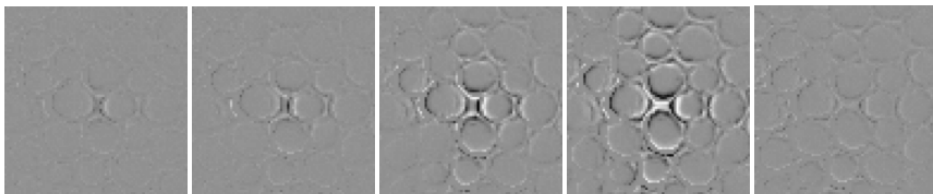
Figure 5.18 – A zoom-in of T1 event as seen in difference of images. The time between frames is 2 seconds. Note the quadrupolar nature of the deformation field.

In Sec. 5.3.1 and Sec. 5.3.2 we show the behavior of dry and wet foams under continuous and start/stop shear, respectively.

5.3.1   Continuous Shear

Using continuous driving, we shear the foam at $v_y = 9.3 \times 10^{-7} ms^{-1}$ for five different packing fractions of $\Delta\phi = 0.025, 0.12, 0.30, 0.54, 0.59$. In Fig. 5.20 we show the traces of the variance (where we now denote $Var := Var[1]$) of these runs, after filtering out the stick-slip motion and performing the affine corrections described in Sec. 5.2.4. The dry foams show short and sharp bursts of motion, the wetter foams at $\Delta\phi \lesssim 0.3$ show increasingly smeared out behavior. Hand in hand with this, the maximal values of the variance decrease for wetter foams. Snapshots of the deformation fields shown in Fig. 5.19 show that the rearrangements for wet foams become more spread out, but also much slower; this explains the lowering of the peaks in Var.
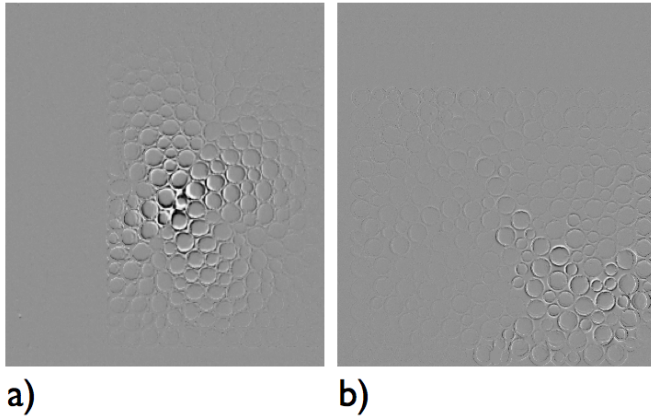
Figure 5.19 – a) A dry foam, mid T1 rearrangement with $\Delta\phi = 0.594$. b) A global rearrangement in a wet foam with $\Delta\phi = 0.025$.
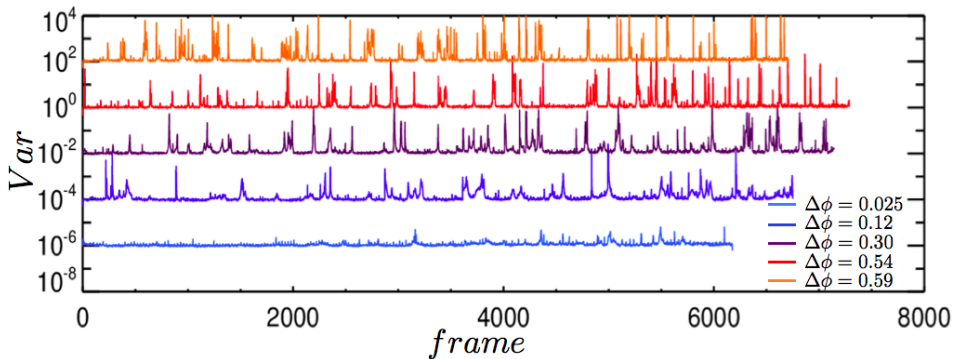
Figure 5.20 – Var versus frame number for five runs, each offset by 10^2 from one another.

A zoom of this data shown in Fig.5.21 clarifies the remarkable differences as we go from a dry to a wet foam. Clearly, runs at low $\Delta\phi$ (blue and light blue) show a low variance signal and deformation events that are drawn out over hundreds of frames. There are fewer sharp peaks in the signal and the system is rarely quiet. This is reminiscent of the nonaffine response seen for systems close to jamming under shear [21, 22]. Increasing the packing fraction to a medium wet foam ($\Delta\phi = 0.30$ (purple)), the behavior starts to change somewhat, with the data showing a mix of sharp peaks and broad ones. The narrowing of the peaks are an indication of the onset of localized rearrangements in the packing, occurring over shorter periods of time. There are still a few global events marked by broad, drawn out rearrangements over tens of frames. The dry foams (red and orange curves

in Fig. 5.21) show only sharp peaks which happen over short periods of time paired with long periods where the system shows no deviations from an affine response.
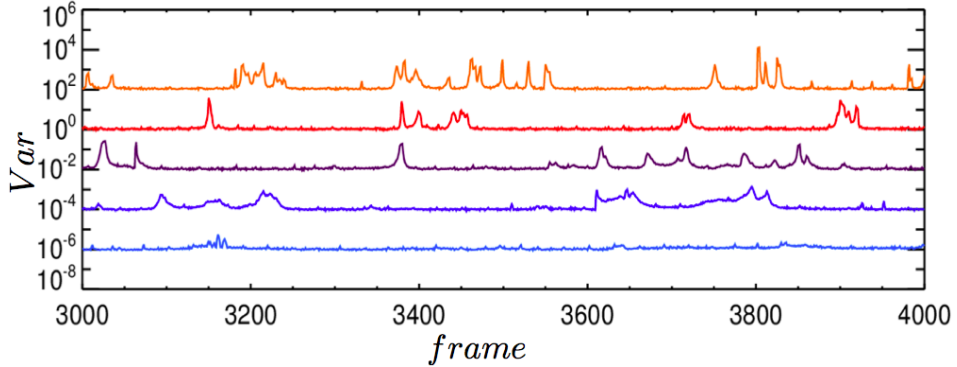
Figure 5.21 – A zoom of the same data in Fig. 5.20, where the packing fractions are $\Delta\phi = 0.59$ (orange), $\Delta\phi = 0.54$ (red), $\Delta\phi = 0.30$ (purple), $\Delta\phi = 0.12$ (blue) and $\Delta\phi = 0.025$ (light blue).

As Fig. 5.21 suggests, a clear distinction between wet and dry foams can be made by looking at the timescales in the variance. To probe this timescale, we have calculated the autocorrelation signal of Var. As the variance, when plotted on a linear scale, is dominated by huge peaks, we focus on the autocorrelation of the log of Var, which we define as:

$$A(\Delta f) := \langle(\log A(i + \Delta f) - \langle\log A\rangle)(\log A(i) - \langle\log A\rangle)\rangle \qquad (5.4)$$

where the average runs over the frame number i and Δf is the change in frame. The result is shown in Fig. 5.22. The autocorrelation thus reveals a systematic lengthening of a characteristic timescale when $\Delta\phi \to 0$. Whether this scale is a strain-scale (i.e. independent of the deformation rate) or is rate dependent is left for further work.
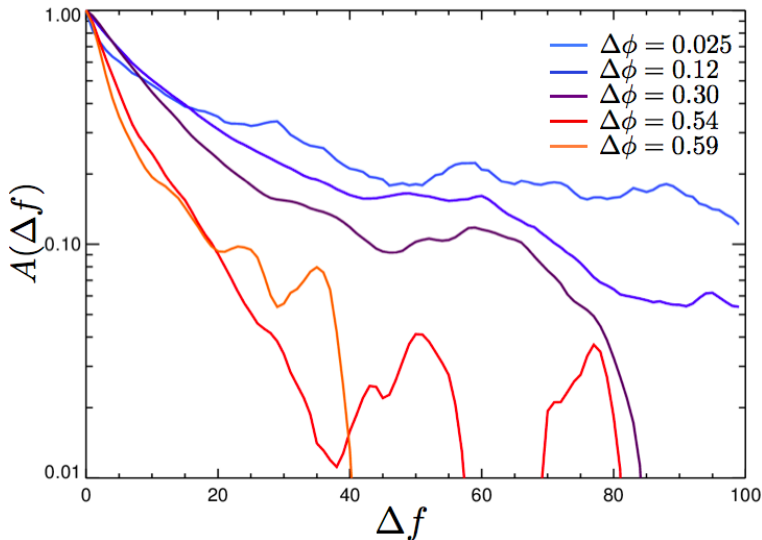
Figure 5.22 – Autocorrelation of $\log(Var)$ versus the change in frame, Δf, for the same five packing fractions shown in Fig. 5.20 and Fig. 5.21.

More quantitative information can be obtained by characterizing the spatial extend of the deformations. To do so, we start from the spatial distribution of the square of the image differences, A^2, see Fig. 5.23.

We then perform some coarse-graining to obtain a 25×25 grid that represents the sum of A^2 over rectangular boxes of a size similar to the bubble size (see right-most image in Fig. 5.23). Denoting these sums as B_{ij}, we define the inverse participation ratio, I_{ipr}, as

$$I_{ipr} := \frac{N \sum_{ij} B_{ij}^2}{\left(\sum_{ij} B_{ij} \right)^2} \, , \tag{5.5}$$

in arbitrary units, where N is the number of boxes (here 625). To interpret the inverse participation ratio, notice that for a homogeneous field where all B_{ij} have the same value, I_{ipr} approaches 1. For an extremely inhomogeneous field, where all but one B_{ij} is zero, $I_{ipr} = N$. Hence, I_{ipr} gives a quantitative measure of the spatial spread of events.

In Fig. 5.24, we show traces and a zoom of I_{ipr} for the five continuous runs we have performed. Similar to the variance signal in Fig. 5.20 and Fig. 5.21, there are more sharp peaks for dry foams than for wet foams, although somewhat surprisingly, the maximal inverse participation ratios in both cases are of order 100.

To clearly distinguish these signals, we now focus on all the local max-
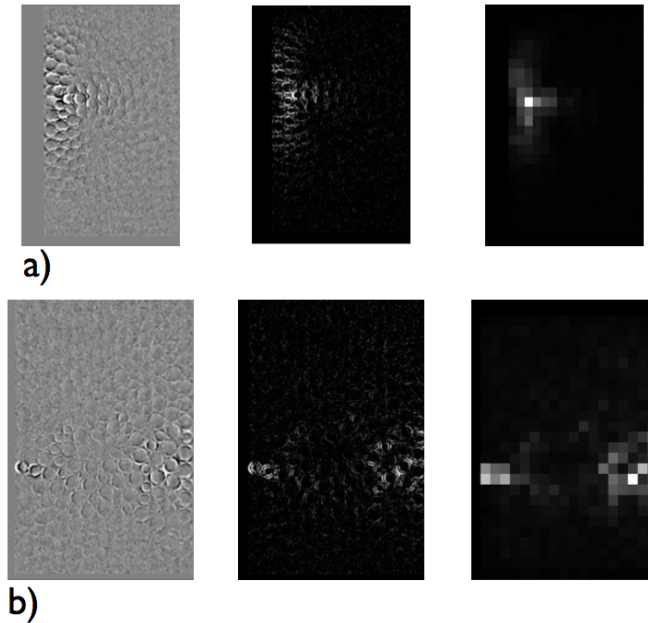
Figure 5.23 – a) Dry foam with $\Delta\phi = 0.54$. From left to right: difference of images, A^2 and sum of A^2 divided over 625 boxes. b) Wet foam with $\Delta\phi = 0.12$.

imum of I_{ipr}. These represent the most localized deformation scales that arise during a deformation.
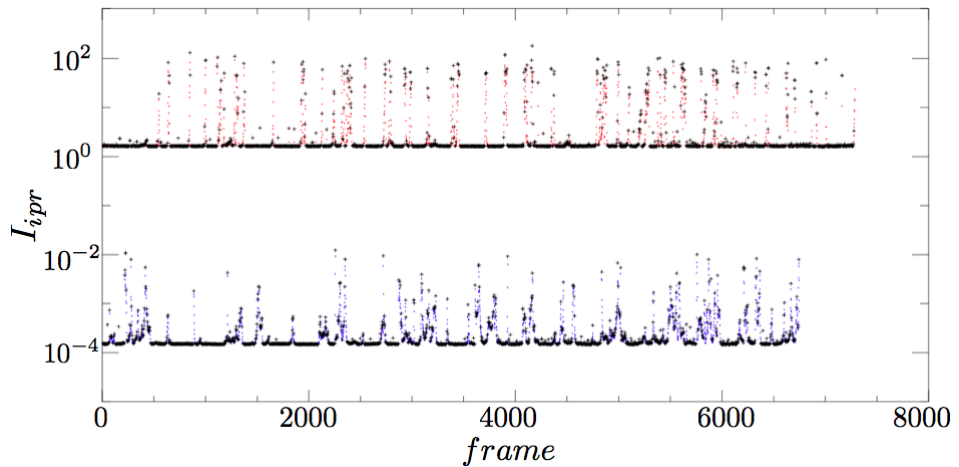
Figure 5.25 – The local maxima of I_{ipr} for two foams with $\Delta\phi = 0.54$ (red) and $\Delta\phi = 0.12$ (blue).
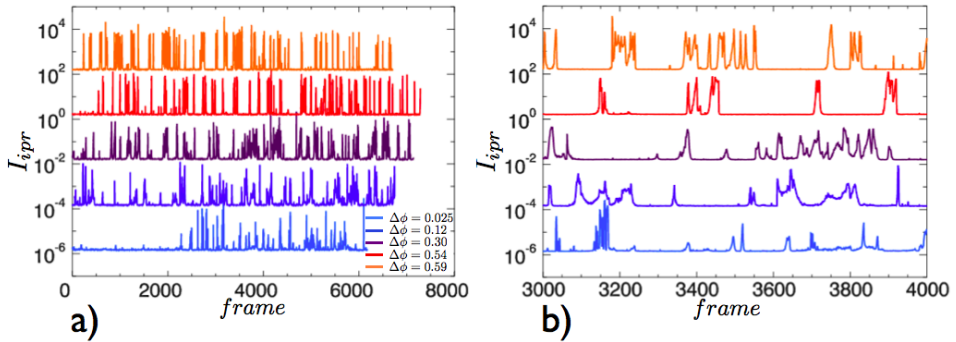
Figure 5.24 – a) I_{ipr} versus frame number for five runs, each offset by 10^2 from one another. b) A zoom of the same data.

Fig. 5.25 shows the traces of I_{ipr} for a wet and dry case, with the maxima marked. A close inspection reveals a qualitative difference between the two: for the dry case, there is an abundance of peaks in I_{ipr} close to the maximum, whereas for the wet case, a wide distribution of local maxima of I_{ipr} can be observed.
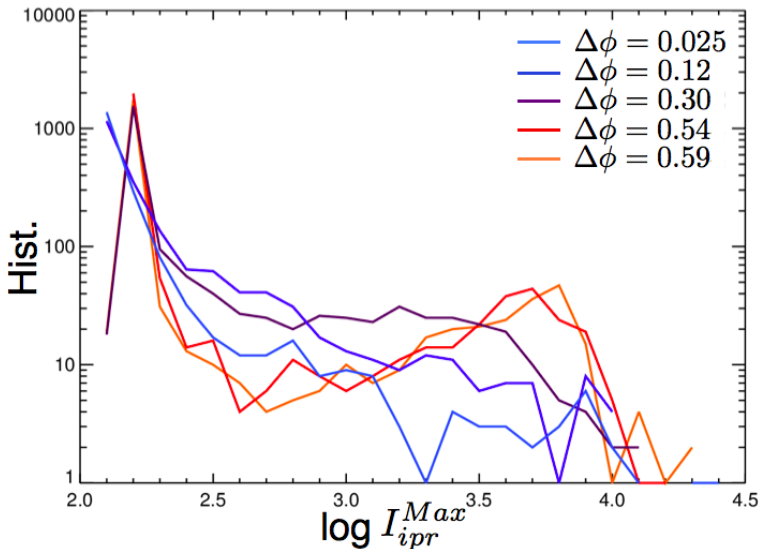
Figure 5.26 – Histogram of $\log I_{ipr}^{Max}$, where I_{ipr}^{Max} are the maxima points identified in Fig. 5.25.

In Fig. 5.26, we show the histogram of the maxima of I_{ipr}, which shows the systematic change from a single to a double-humped distribution as the packing fraction $\Delta\phi$ is increased. We interpret the second peak for the
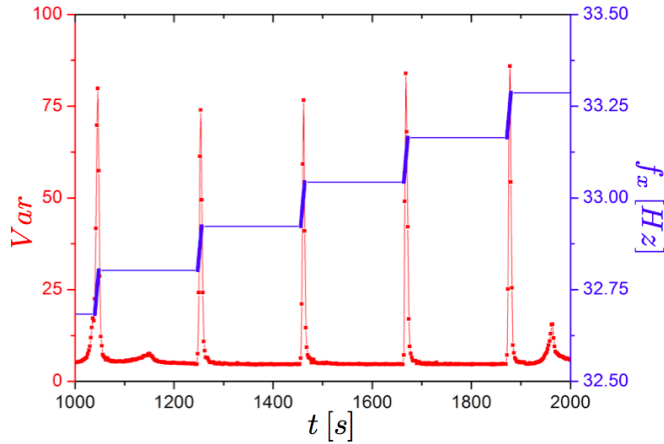
Figure 5.27 – Var (red) and f_x (blue) versus time for a start/stop run with $\Delta\phi \approx 0.25$ and $t_c = 8\,s, t_s = 200\,s$. The peaks in the variance show that the walls are moving.

dry foams as corresponding to T1 events, and the loss of this peak again illustrates the loss of relevance of such localized rearrangements closer to jamming.

5.3.2 Start/stop Shear

Using the start/stop protocol, we have explored the variance in order to probe the temporal evolution of the system during the sit time, t_s. In particular, we are interested in how the system relaxes the internal stress by rearrangement due to the shear.

Fig. 5.27 shows Var and driving rate f_x versus time for a medium wet foam of $\Delta\phi \approx 0.25$ for a start/stop run with $t_c = 8\,s, t_s = 200\,s$. The walls move only a short time, yet enough for a noticeable variance signal to be detected. The steps in f_x as seen in Fig.5.27 thus create periodically-spaced peaks.

In Fig. 5.28, Var versus time for three different packing fractions of $\Delta\phi \approx 0.15, 0.25, 0.45$ is shown over $t_s = 200\,s$. In all three examples, deformations are taking place during the sit time. For the dry case in Fig. 5.28 a), rearrangement events occurs over a relatively short period of time, as expected, yet the variance signal is not as strongly peaked, in contrast to Fig.5.21 in Sec.5.3.1, where T1 events in a dry foam were marked by sharp peaks. We note that in the continuous shear case, T1 events were of much shorter duration, which partially explains this difference. As we approach the wet foam in Fig. 5.28 b) and c), Var increases in magnitude

113

and the events take longer to subside. The larger variance signal indicates more bubbles partaking in motion. This larger variance is, however, in contrast to the wet foam behavior seen in continuous shear, where the wet foams exhibited low variance signals(see Fig. 5.21).
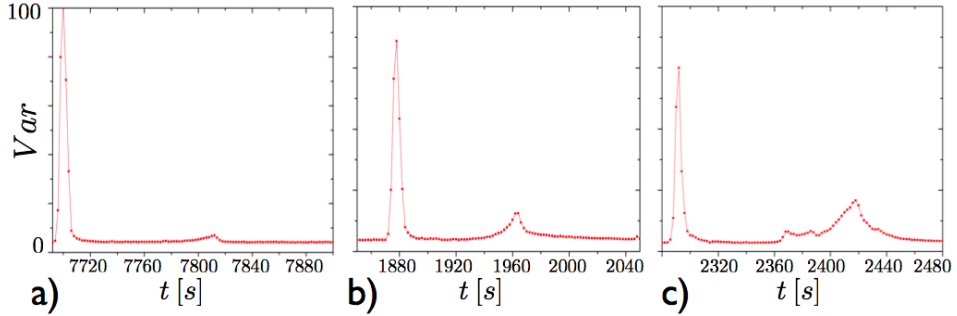
Figure 5.28 – Var versus time for a) $\Delta\phi \approx 0.45$, b) $\Delta\phi \approx 0.25$, and c) $\Delta\phi \approx 0.15$ with $t_c = 8\,s, t_s = 200\,s$.

Var in Fig. 5.28 c) also highlights the continuity of motion in wet foams in that separate rearrangement events seemed to be linked. Between 2360 and 2400 seconds, the motion starts with only a few bubbles partaking, as shown by the low variance. The variance signal then grows rapidly, before eventually relaxing completely. This behavior is an indicator of avalanches in wet foams, meaning one event can "trigger" a further deformation in the packing.
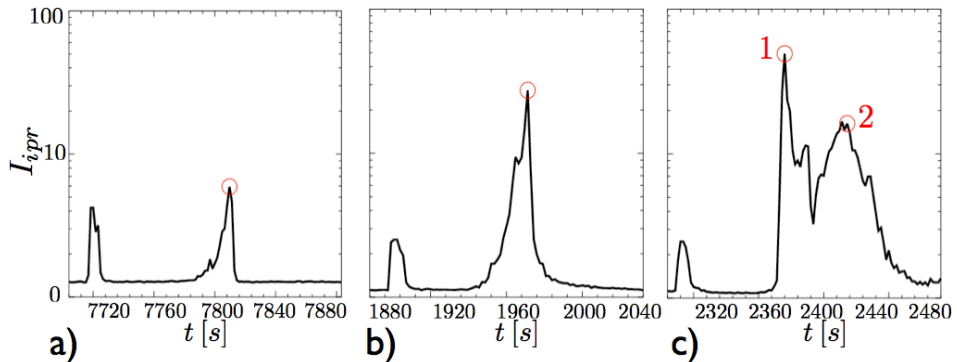
Figure 5.29 – I_{ipr} versus time for a) $\Delta\phi \approx 0.45$, b) $\Delta\phi \approx 0.25$, and c) $\Delta\phi \approx 0.15$ with $t_c = 8\,s, t_s = 200\,s$.

To understand the change in behavior between continuous and start/stop shear, we show the I_{ipr} versus time for the three packing fractions in Fig. 5.29. The T1 event identified in Fig. 5.28 a) for the dry foam shows a

relatively low value in the inverse participation ratio in Fig. 5.29 a) compared to the wetter foams. This is due in part to the signal noise from the periods when the foam is not deforming overwhelming the T1 signal in I_{ipr}, see Fig. 5.30 a). As $\Delta\phi \to 0$ in Fig. 5.29 b) and c), the I_{ipr} signals broaden similar to Fig. 5.26, indicating a departure from localized behavior to more global deformations in the foam. This is further illustrated in Fig. 5.30, where the difference of images correspond to the circled peaks in Fig. 5.29.
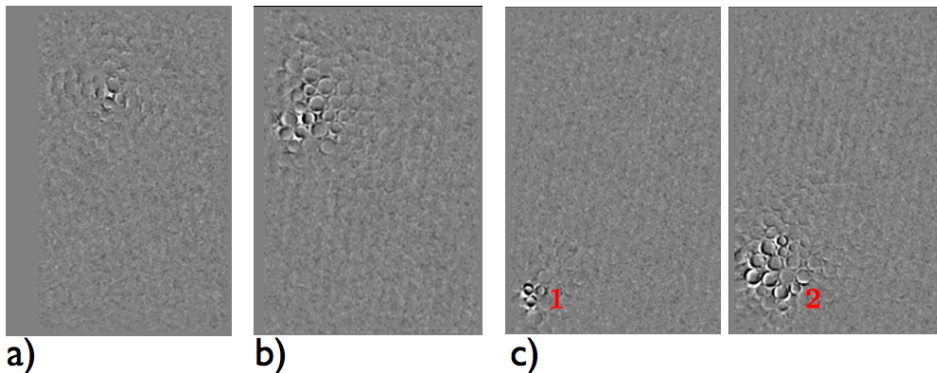
Figure 5.30 – Difference of images of the red-circled peaks from Fig. 5.29 with a) $\Delta\phi \approx 0.45$, b) $\Delta\phi \approx 0.25$, and c) $\Delta\phi \approx 0.15$. The two peaks in c) show at first localized behavior and then more broad, global deformations.

5.4 Conclusions and Outlook

We have shown that a two-dimensional foam under pure shear exhibits markedly different behavior in the wet and dry case, both spatially and temporally. First, the autocorrelation shown in Fig. 5.22 reveals a systematic lengthening of a characteristic timescale when $\Delta\phi \to 0$. Secondly, histograms of the inverse participation ratio (Fig. 5.26) show that only very dry foams show localized T1 events via a peak in the histogram for large values of I_{ipr}. The loss of this peak when $\Delta\phi \to 0$ illustrates the loss of localized behavior as we approach jamming.

What remains to be investigated is what is driving the rearrangements in the foam. Does one rearrangement necessarily trigger another? What is the role of coalescence events and coarsening? What causes rearrangements long after driving has ceased?

Moreover, the lengthening of the timescale observed as a foam becomes wetter in Fig. 5.22 remains to be investigated further. The question of whether there is a rate (in)dependence of the rearrangements on the shear

rate was touched upon briefly in [33, 63]. If the shear rate is decreased (increased), it is yet unclear whether the rate of rearrangement will also slow (speed up). For fast events, as in dry foams, we expect the shear rate to be inconsequential; we believe events to appear similarly for fast and slow shear rates. For intrinsically slow deformations, as in wet foams where the motion is more global, we expect the shear rate to play an important role for the rearrangement.